Design of Wideband, Circularly Polarized Patch Antennas for RFID Applications in the FCC/ETSI UHF Bands

Marios Nestoros[1], Marios A. Christou[2], and Anastasis C. Polycarpou[1, *

Abstract—The primary objective of this paper is to design a high-gain, circularly polarized patch antenna suitable for Radio Frequency Identification (RFID) readers that operate in the FCC and ETSI bands (865–928 MHz). These designs will be used in a healthcare application to provide tag identification for thousands of medicines stored on shelves inside a pharmaceutical warehouse. Consequently, it is important that these antennas provide sufficient electromagnetic coverage and polarization diversity in order to boost tag readability and minimize item identification errors. The proposed RFID reader antenna design begins with a single patch with truncated corners on air substrate in order to help us understand the effect of various geometrical parameters on critical antenna figures of merit. A stub is introduced in order to improve the impedance matching characteristics of the antenna. The wideband characteristic of the design, for both impedance matching and axial ratio, is achieved by a second truncated-corner patch antenna positioned on top of the first one. An optimum design is achieved by changing the heights of the main and parasitic patches, the size of the truncated corners, and the probe position. The final antenna designs are verified by comparing measurement and simulation results.

1. INTRODUCTION

The emergence of RFID technology in recent years finds numerous applications in today's society including identification of objects, people and animals, baggage localization and tracking at airports, logistics and supply chain management, library management systems (LMS), real time localization systems (RTLS), security systems, the internet of things (IoT), industrial automation, and many more [1]. The effectiveness of a passive RFID system for a given application strongly depends on electromagnetic (EM) coverage, polarization diversity, and tag sensitivity. The first two attributes have to do with the design of the reader antennas, as well as the design of the antenna network in a realistic environment. Consequently, it is important that the reader antennas exhibit good radiation characteristics including impedance matching, axial ratio, gain, and radiation patterns within the frequency band of interest. In this paper, our objective is to use basic antenna design techniques, starting with a simple design and moving to a more complex but more effective design, in order to understand the parameters affecting the most important antenna figures of merit. The resulting antenna designs will be used in an RFID project related to healthcare [2]. Specifically, in the context of a running project, we would like to design the antenna element itself as well as the network of antennas inside a pharmaceutical warehouse where thousands of medicines are stored. In this work, we will focus on the antenna design which has to be wideband, in order to cover both ETSI and FCC bands, as well as circularly polarized.

The basic design principle originates from a paper by Sharma [3] who was the first to analyze computationally the truncated-corner patch on low dielectric-constant substrates. Such a topology could be optimized in order to provide circular polarization at the center frequency of interest. Specifically, the

* Corresponding author: Anastasis C. Polycarpou (polycarpou.a@unic.ac.cy).
[1] Department of Engineering, University of Nicosia, Cyprus. [2] Department of Mathematics, University of Nicosia, Cyprus.

ratio of the truncation size over the length of the square patch can be judiciously chosen in order to obtain a very low axial ratio at the center frequency. The design procedure, however, is not straightforward and, as we will see later on, other parameters affect the optimum design. The drawback of this particular single-patch design, based on truncated corners, is that the axial-ratio bandwidth, as well as the impedance bandwidth, is very narrow. Consequently, researchers in the last two decades have worked on various patch antenna topologies in order to enhance axial-ratio and impedance bandwidths, in addition to other important antenna characteristics. One such design, which was used for a UHF RFID reader, is the introduction of a semicircular slot into the main circular radiating patch [4]. The impedance and axial-ratio bandwidths were optimized using the L-shaped probe-fed approach. The particular design though is suitable only for the FCC RFID band and incorporates FR4 substrates which further reduce antenna efficiency. In addition, the height of the antenna is a bit larger than 32 mm which mandates a bulkier enclosure. A wideband patch antenna design for RFID reader applications was recently achieved by Jian Li et al. [5]. They specifically used two feeding lines with quadrature phase difference to excite the lower circular patch at two points. A parasitic circular patch is placed on top of the main radiating patch, whereas both of them are shorted in the center. This particular design exhibits a high gain and antenna efficiency as it does not incorporate lossy dielectrics. Its drawback is the use of a feeding network which occupies additional significant space in the antenna enclosure. In addition, this feeding network may create asymmetries in the radiation patterns of the antenna. Another wideband design is the work by Chen et al. [6] who demonstrated a universal UHF RFID reader antenna that operates in both FCC and ETSI bands. The simulated and measured axial ratio is lower than 3 dB within the band of interest, whereas the gain of the antenna was found to be 8.3 dBic. The disadvantage of this particular design was the complexity of the geometry and the relatively large height of the antenna (35 mm), which requires a larger enclosure. Another interesting RFID reader antenna design is the one published by Sim et al. [7] using truncated corners and slits on the patch. This particular design is a single layer patch antenna printed on an FR4 substrate and an L-shape ground plane. The return loss and axial ratio satisfy the antenna design requirements for the entire band and the gain is found to be 8.6 dBic. The disadvantage of this antenna is the extremely large height of the patch from ground (60 mm) which makes the antenna packaging very bulky.

The objective of the current work is to achieve enhanced axial-ratio and impedance bandwidths, as well as high gain and high beamwidth symmetric radiation patterns, using a single-feed approach. As known, a single-fed circularly polarized single-patch antenna has the disadvantage to exhibit narrow impedance bandwidth and narrow axial-ratio bandwidth, which is often less than 2% [8, 9]. One approach to enhance both types of bandwidth is through use of thick substrates [10], which tend to support strong surface waves, and consequently, diffraction by the edges of the ground plane resulting in strong back radiation. Other approaches include use of shorting pins or alternative feeding mechanisms [4, 11, 12], parasitic elements [13–15], or even metasurfaces [16].

The novelty of this work is twofold. First, we identified the effect of the individual geometrical parameters (e.g., main and parasitic patch heights, corner truncation, stub length/width, etc.) on the antenna characteristics, and how these may be adjusted in order to achieve an optimum design without numerous simulations. Second, the final design is characterized by wide bandwidth for both axial ratio and input impedance without use of a two-line feeding network and geometrical asymmetries which have a negative impact on radiation patterns. In addition, we avoided using substrates (e.g., FR4) in order to eliminate dielectric losses, thus boosting antenna gain and efficiency to a maximum value.

Two individual antenna designs are presented in the following section: a single-patch narrowband antenna and a double-patch wideband antenna. The designs were optimized using a series of parametric studies based on ANSYS HFSS commercial software, and they were verified based on experimental results obtained in the laboratory.

2. ANTENNA DESIGN METHODOLOGY AND RESULTS

The design procedure started with simple square patch antenna designs on air substrates incorporating geometrical modifications, such as truncated corners and stubs, in order to optimize critical antenna figures of merit. Correlation of geometrical modifications with antenna characteristics was identified and noted in the context of multiple parametric studies. An open-circuited stub was also introduced
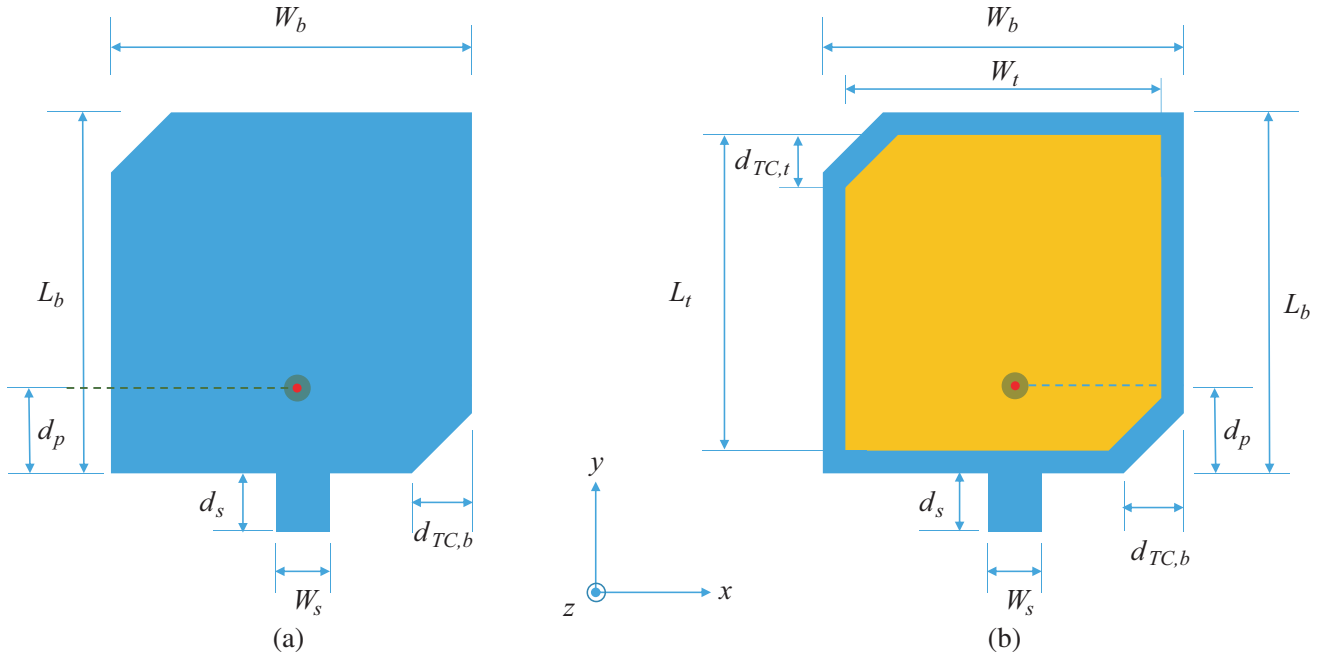
Figure 1. Geometry of the truncated-corner patch. (a) Single patch with a probe feed and an open-circuited stub in the vicinity of the probe; (b) Stacked truncated-corner patches with a probe feed on the bottom patch and an open-circuited stub attached to the bottom patch in the vicinity of the probe.

in order to enhance Voltage Standing Wave Ratio (VSWR) performance within the bandwidth of interest. Stacked patches were used in order to improve Return Loss (RL) and Axial Ratio (AR) bandwidths. Fig. 1(a) illustrates the basic geometry of the single-patch antenna adopted in the study which incorporates truncated corners, an open-circuited stub and a 50-Ω coaxial feed attached to the patch from underneath. Fig. 1(b) illustrates the geometry of a stack of two truncated-corner square patches which was introduced in order to enhance bandwidth that sufficiently covers both ETSI and FCC UHF RFID bands.

The initial design begins with the calculation of the width of the patch that supports good radiation efficiency [17]

$$W = \frac{c}{2f_r}\sqrt{\frac{2}{\epsilon_r + 1}} \tag{1}$$

where c is the free-space speed of light, f_r the desired resonance frequency, and ϵ_r the dielectric constant of the substrate, which is unity in our case as the material between the conducting patch and ground is air. As a result, the effective dielectric constant, ϵ_{reff}, will be unity as well. Once W is obtained, the actual length of the patch is given by

$$L = \frac{c}{2f_r\sqrt{\epsilon_{reff}}} - 2\Delta L \tag{2}$$

where

$$\Delta L = 0.412h\frac{(\epsilon_{reff} + 0.3)\left(\dfrac{W}{L} + 0.264\right)}{(\epsilon_{reff} - 0.258)\left(\dfrac{W}{L} + 0.8\right)} \tag{3}$$

Assuming that h ranges between 6 mm and 12 mm, the calculated value of L comes close to 163 mm. As a starting design, we chose the length and width of the patch to be 160 mm.

2.1. Single-Patch Antenna — Simulation Results

The aim of the first series of simulations, using ANSYS HFSS, was to optimize the single-patch design on an air substrate by varying the 45-degree corner truncation distance $d_{TC,b}$, the position of the coaxial probe d_p with respect to the edge, and the height of the patch antenna above the ground plane, h. Initially, the design assumed no stub, whereas the ground plane was set to $200 \times 200 \, \text{mm}^2$. Our main objective was the design of a circularly-polarized patch antenna with single feed that operates in the ETSI UHF band (865–868 MHz) and exhibits high gain, low VSWR and AR close to unity (0 dB). In addition, we seek insight into the single-patch design procedure, as well as understanding of the influence of the various geometrical parameters on important antenna characteristics. The performance of the different designs over the frequency band of interest was evaluated based on the S_{11}, VSWR, AR and Gain (G).

The AR and S_{11} are shown in Fig. 2 for the case of $45°$ corner truncation, which was optimal in regard to the AR. The size of the patch was $160 \times 160 \, \text{mm}^2$, the height was $h = 12 \, \text{mm}$, and the probe position was $d_p = 40 \, \text{mm}$. The size of the truncated corner, $d_{TC,b}$, was the variable parameter changing from 16 mm to 26 mm. From Fig. 2(a), it is evident that by increasing the size of the truncated $45°$ corners of the patch, the AR improves gradually reaching 0 dB for the case of $d_{TC,b} = 26 \, \text{mm}$. A similar type of improvement occurs for the case of S_{11} versus frequency, as shown in Fig. 2(b). By increasing the size of the truncated corners, the S_{11} gradually improves to lower than $-30 \, \text{dB}$. The main problem though is the fact that the optimum AR occurs at 840 MHz whereas the optimum S_{11} occurs at 880 MHz. Both these distinct frequencies are outside the ETSI UHF RFID band of interest, which is 865–868 MHz.
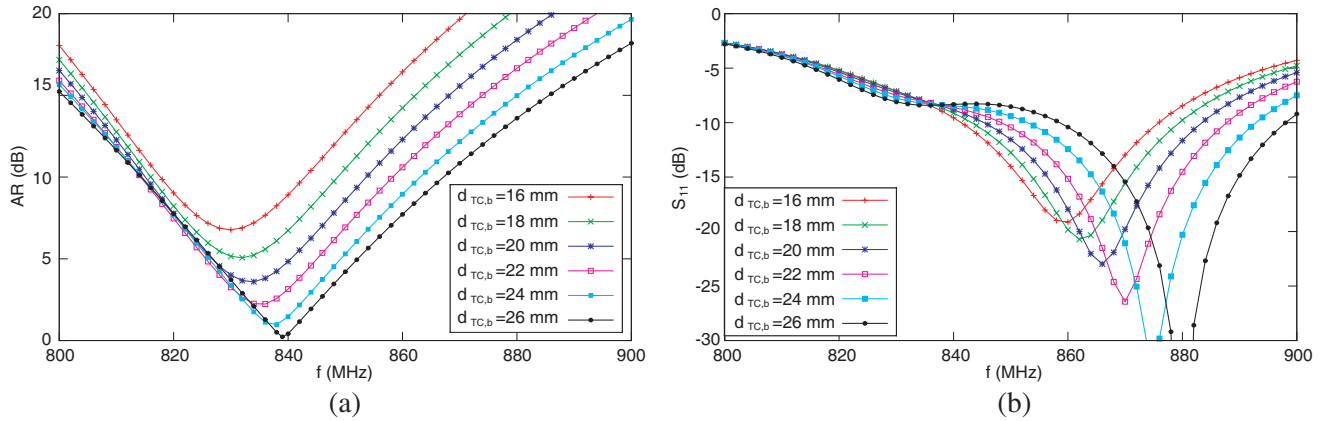
Figure 2. Single patch $(160 \times 160 \, \text{mm}^2)$ without stub on an air substrate at $h = 12 \, \text{mm}$ above ground $(200 \times 200 \, \text{mm}^2)$; the probe is located at $d_p = 40 \, \text{mm}$. (a) Axial Ratio as a function of frequency for different values of truncated-corner size. (b) S_{11} as a function of frequency for different values of truncated-corner size.

In order to shift the optimum (0 dB) AR to a higher frequency (e.g., 865 MHz), the height of the patch — measured from the ground plane — was reduced. By decreasing the height, it was observed that the minimum value (not necessarily the optimum one) of the AR moves to higher frequencies. For an optimum value of 0 dB in AR, the size of the corner truncation had to be judiciously chosen. Fig. 3(a) illustrates two cases: one for $h = 6 \, \text{mm}$, where the AR becomes 0 dB at 872 MHz, and one for $h = 7 \, \text{mm}$, where the AR becomes 0 dB at 862 MHz. Both these 0 dB values in AR were achieved through optimization of the design by changing the size of corner truncation. The corresponding truncation size for these two cases is 18 mm. However, from Fig. 3(b), it is evident that S_{11} barely satisfies the $-10 \, \text{dB}$ impedance matching criteria, even though the RL bandwidth is very good.

Improvement of the impedance matching characteristics of the single-feed, truncated-corner, single-patch antenna over a ground plane can be achieved through the use of a microstrip stub which is placed close to the probe location, as shown in Fig. 1(a). The microstrip stub is centered along the side of
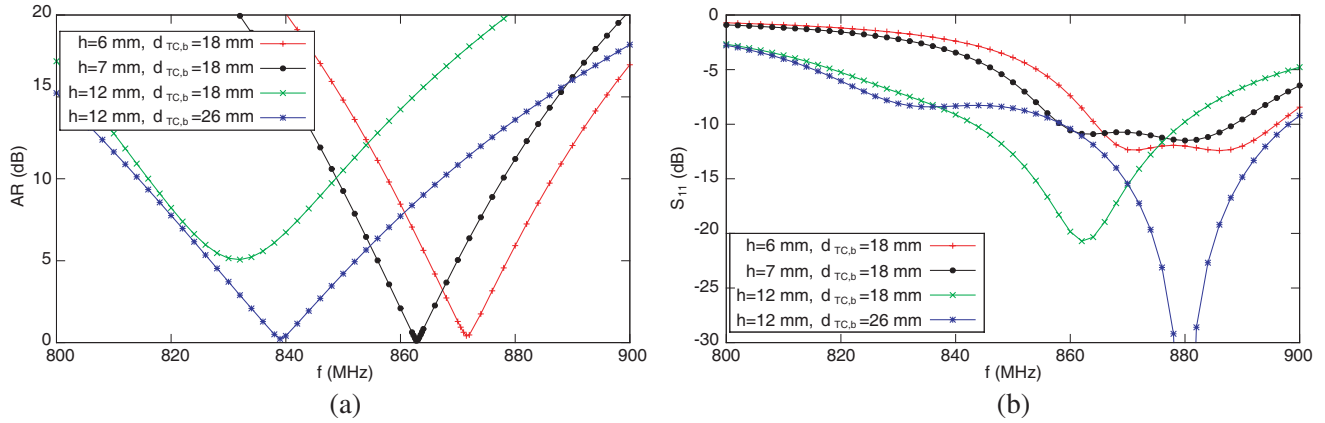
Figure 3. Optimizing antenna performance based on the Axial Ratio and S_{11}. (a) Axial Radio (in dB) versus frequency for different heights and truncated-corner size. (b) S_{11} (in dB) versus frequency for different heights and truncated-corner size.
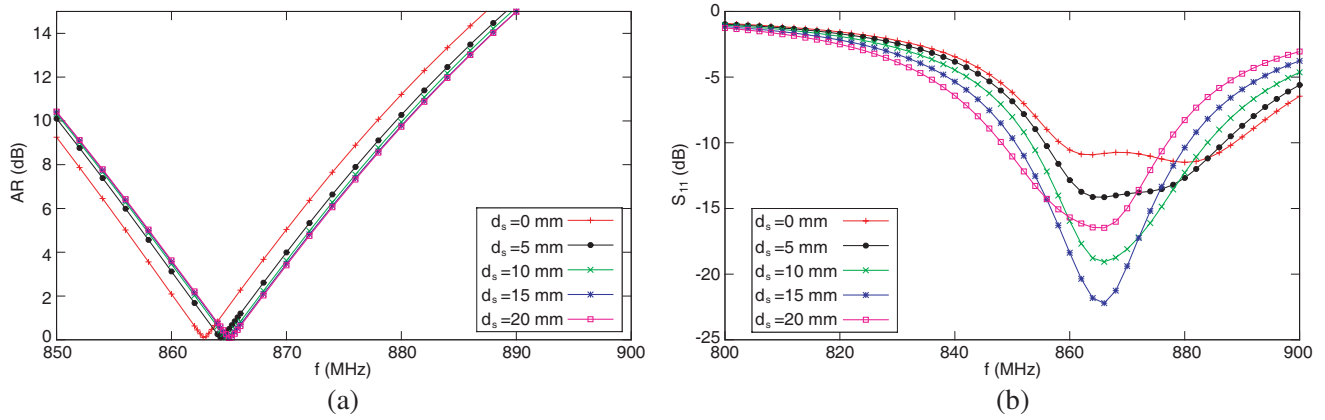
Figure 4. Tuning the S_{11} by varying the stub length ($W_s = 20\,\text{mm}$, $h = 7\,\text{mm}$). (a) Axial Radio (in dB) versus frequency for different lengths of the centered stub. (b) S_{11} (in dB) versus frequency for different lengths of the centered stub.
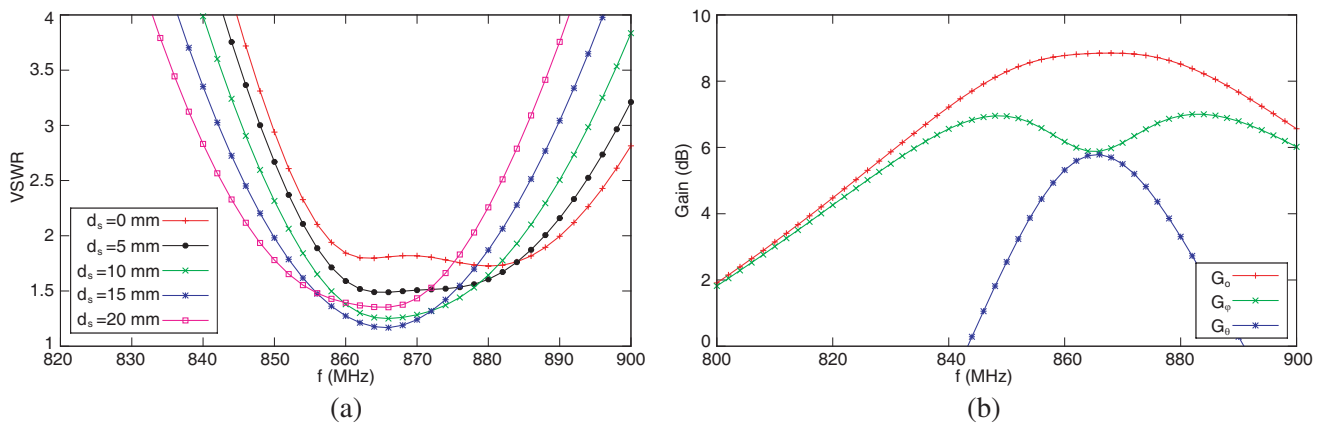
Figure 5. (a) VSWR versus frequency for different lengths of the centered stub ($W_s = 20\,\text{mm}$, $h = 7\,\text{mm}$). (b) Realized gain (in dBi) versus frequency of the optimum antenna design that corresponds to $d_s = 15\,\text{mm}$, $W_s = 20\,\text{mm}$, and $h = 7\,\text{mm}$.

the patch and extends to a distance away from the edge equal to d_s. Fig. 4 illustrates the influence of the length of the stub on the AR and S_{11}, which are plotted as a function of frequency. For all cases illustrated, the width of the stub was $W_s = 20$ mm. As shown, the length of the stub has a pronounced effect on the S_{11} of the antenna and a much smaller effect on the frequency response of the AR. Specifically, by increasing the length of the stub, the S_{11} of the antenna improves to a value beyond -20 dB when $d_s = 15$ mm. Further increase of the stub length does not cause additional improvement. From Fig. 4(a), it is evident that the frequency response of the AR shifts to a bit higher frequencies by increasing stub length. Consequently, for $d_s = 15$ mm, the AR becomes precisely 0 dB at a frequency of 865 MHz. The AR remains smaller than 3 dB for the entire UHF RFID ETSI band.

The corresponding VSWR and realized gain of the antenna as a function of frequency are depicted in Fig. 5. As illustrated, the optimum antenna design with a single feed and a microstrip stub results in a VSWR that is lower than 2 for the entire UHF RFID ETSI band. In addition, the maximum total realized gain of the optimum design was 8.85 dBi. This maximum realized gain occurs at the center of the UHF RFID ETSI band. It is also interesting to observe from Fig. 5(b) that the two components of the realized gain, e.g., G_θ and G_ϕ, are equal at the center of the frequency band of interest, implying a circularly polarized antenna.

2.2. Single-Patch Antenna — Measurements

The simulation results for S_{11}, AR and radiation patterns were verified against measurements performed in the Radio-Communications Laboratory of the University of Nicosia. The fabricated single-feed, single-patch antenna with an open matching stub is illustrated in Fig. 6. The antenna was made of aluminum sheet using a CNC router. The patch was fixed on the ground plane using nylon posts, as shown in the picture. The measurements for S_{11} were made on an ADVANTEST R3132 scalar Spectrum Analyzer in conjunction with an HP dual directional coupler (775D) and terminating loads, as shown in Fig. 7. The comparison between HFSS simulations and measurements are depicted in Fig. 8. As illustrated, the agreement between the two sets of data is fairly good. There is a slight shift in the resonance frequency toward lower frequencies. Initially, this was thought to be attributed to fabrication tolerances observed on the etching of the patch using the CNC router. However, after close examination of the fabrication process, it was deduced that minor geometrical discrepancies equivalent to fractions of a millimeter do not have such an impact on the resonance frequency of the antenna. Further investigation had shown that this single-patch antenna design is very sensitive to the height from the ground, which cannot be set precisely. As observed from Fig. 8, by slightly decreasing the height of the patch by even 1 mm, the resonance frequency shifts by approximately 30 MHz to higher frequencies. As a result, a single-patch design is highly sensitive to the height of the patch from the ground, and thus, depending on the accuracy of the fabrication process, the resonance frequency may be shifted outside the desirable frequency band. Nevertheless, it is important to notice that the S_{11} bandwidth, depth and shape of the measured frequency response closely resemble those obtained from the ANSYS HFSS simulation.

Similar observation is noted for the AR frequency response where the optimum circular polarization

(a)   (b)
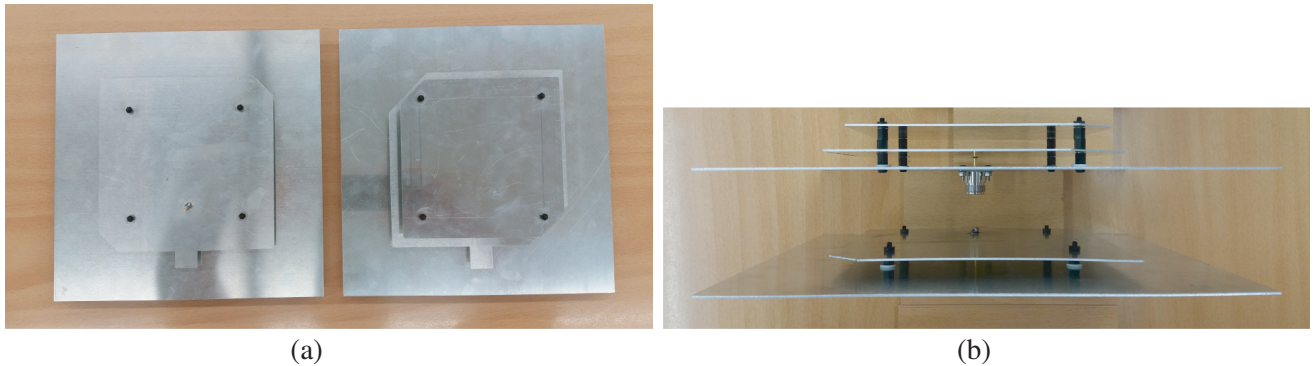
Figure 6. Fabricated single- and double-patch antennas. (a) Top View; (b) Side View.

(a)   (b)

Figure 7. Measurement setup for the single-patch antenna. (a) Spectrum analyzer and directional coupler; (b) Spectrum analyzer, directional coupler and antenna.

(a)   (b)
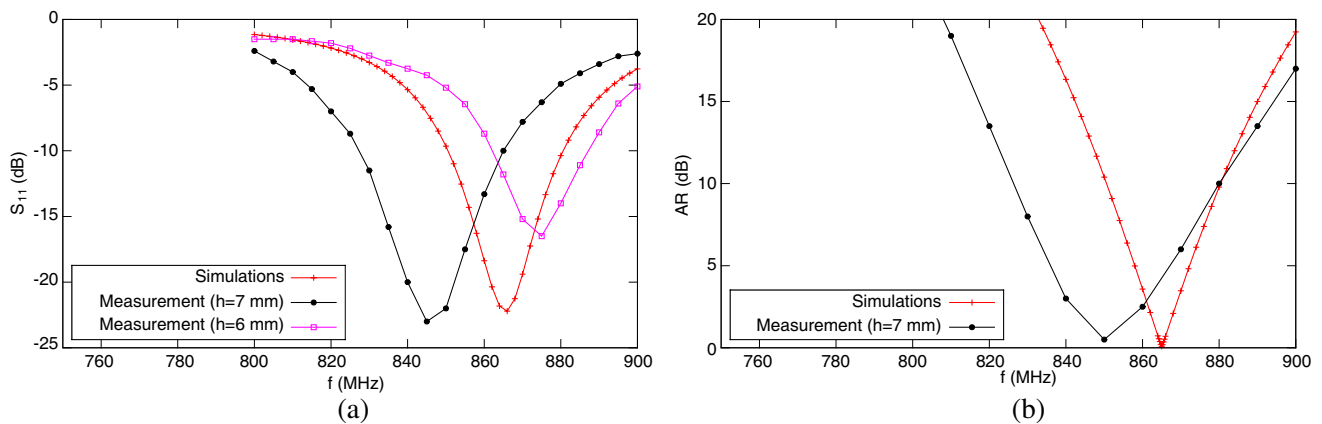
Figure 8. Comparisons between HFSS simulations and measurements. (a) S_{11} versus frequency; (b) AR versus frequency.

is observed approximately 20 MHz lower than that of the simulated results. The reason for the slight shift in frequency is attributed to fabrication tolerances concerning the precise height of the patch from the ground. As discussed earlier, the resonance frequency of the single-patch antenna is highly sensitive to height variations. Furthermore, the measurements of all the antenna characteristics were performed in a non-anechoic room, thus the radiated fields were susceptible to unwanted scattering by the ground and surrounding walls of the laboratory, even though an extra effort was placed to reduce such interferences. The E_ϕ and E_θ components of the normalized radiated field at the resonance frequency, along the E- and H-planes, respectively, is depicted in Fig. 9. As illustrated, there is a good agreement between measurements and simulations despite the fact that the experiments were performed in a non-anechoic chamber. During measurements, we placed absorbers on the ground and positioned the transmitting/receiving antennas far away from walls and other obstacles in order to minimize the effects of stray scattering.

In addition to the radiation patterns, we also calculated the overall efficiency of the single-patch antenna. According to [17], the overall antenna efficiency is a product of three individual efficiency components: conduction efficiency (η_c), dielectric efficiency (η_d), and reflection efficiency (η_r). In our case, the conduction efficiency is unity as we are assuming perfect electric conductors for the patch and
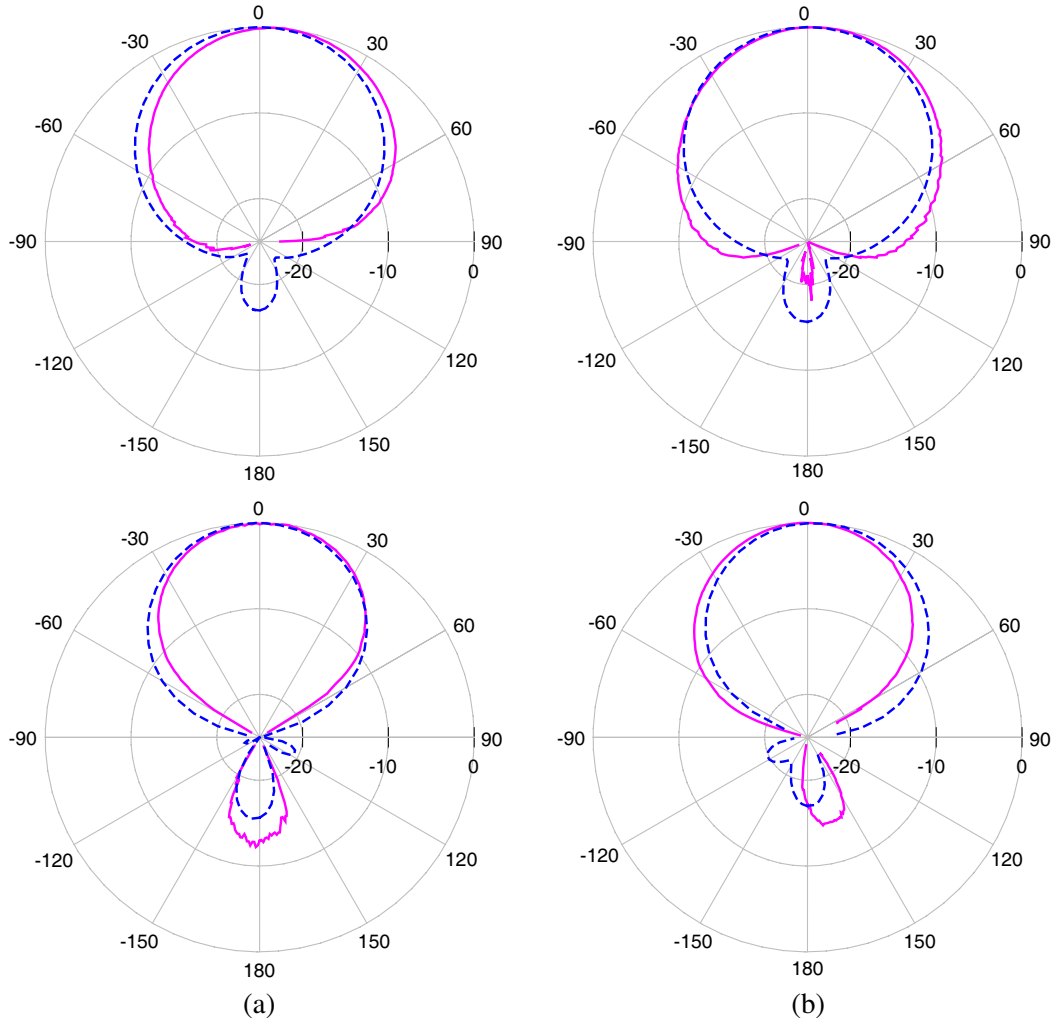
Figure 9. Comparisons between simulations (dash blue line) and measurements (solid purple line) for the normalized radiations patterns (Top: E_ϕ; Bottom: E_θ) in the E- and H-planes at the resonance frequency of the single-patch antenna. (a) E-plane elevation pattern (z-y plane); (b) H-plane elevation pattern (z-x plane).
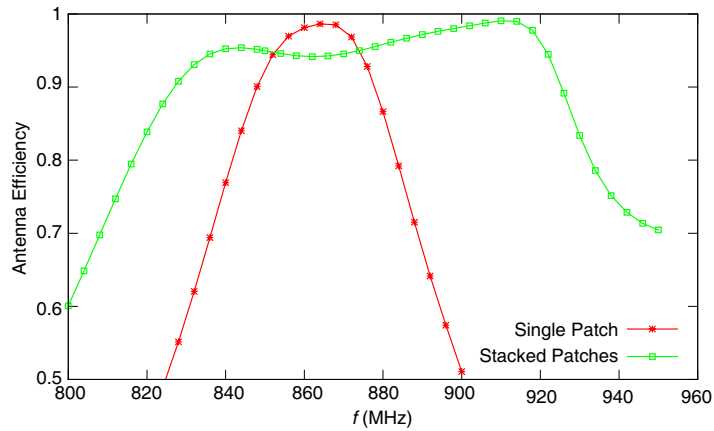
Figure 10. Antenna efficiency for the single-patch and stacked-patch antennas.

ground plane. The dielectric efficiency is also unity as there is no dielectric material; in other words, the patch is suspended in air using nylon posts. Therefore, the overall antenna efficiency will be equal to the reflection efficiency, which is defined as the accepted power over the input power. The antenna efficiency of the single-patch antenna was computed and plotted in Fig. 10. As seen, the antenna efficiency curve is centered around the middle of the RFID ETSI UHF band. In addition, the efficiency approaches unity in the middle of the band due to the fact that there are no dielectric losses, which are usually observed in substrates such as FR4.

2.3. Stacked-Patch Antenna — Simulations and Measurements Results

As observed from the aforementioned analysis and experiments, a single-feed, single-patch antenna may be carefully designed in order to obtain optimum antenna characteristics within a very narrow frequency band. However, its frequency response is highly sensitive to small changes in the height of the patch from the ground. Consequently, the fabrication process has to follow very strict guidelines in order to avoid shifting of the resonance to lower or higher frequencies outside the narrow band of interest.

This drawback, inherent to the particular single-patch design, could be avoided if a wideband antenna is designed instead. In order to achieve such a design, we incorporated a stack of two patches with truncated corners and slightly different dimensions. The geometry of this design is illustrated in Fig. 1(b). Such a design must be optimized for all major antenna characteristics, including AR and S_{11}. The particular antenna design must exhibit wideband response for AR and S_{11} covering both ETSI and FCC UHF RFID bands.

Following a series of parametric studies by altering either the height of the two patches, or the truncation size of each patch, or the dimensions of the two patches, or the probe feed position, the optimum design that satisfies both AR and S_{11} wideband characteristics is shown in Table 1. As illustrated the upper patch has smaller dimensions than the bottom patch, the corner truncation size is different, and the probe is attached only to the lower patch (single feed). It is obvious from Fig. 11

Table 1. Specifications for the stacked-patch antenna design. Units are in mm.

Description	Patch Dimensions $(L \times W)$	Corner Truncation (d_{TC})	Patch Height (h)	Probe Location (d_p)	Center Stub $L_s \times W_s$
Lower Patch	160×160	36	7	15	20×20
Upper Patch	142×142	21	19	–	–
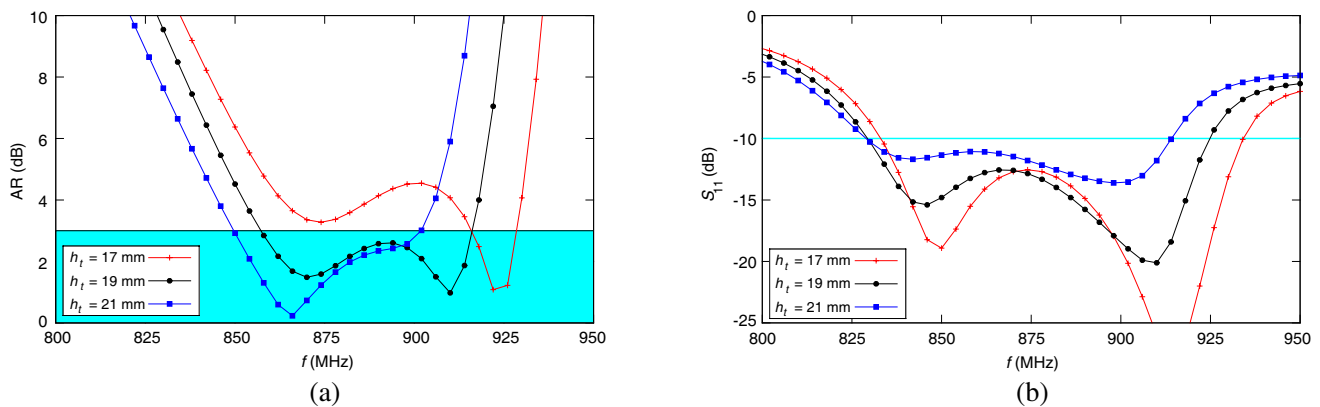
Figure 11. Parametric studies. (a) AR versus frequency for different heights of the top patch. (b) S_{11} versus frequency for different heights of the top patch. ($W_s = L_s = 20$ mm, $h_b = 7$ mm, Bottom patch: 160×160 mm^2 and $d_{TC,b} = 36$ mm; Top patch: 142×142 mm^2 and $d_{TC,t} = 21$ mm).

that both AR and S_{11} wideband criteria for a proper antenna design can be satisfied with the judicious choice of the aforementioned geometrical parameters. As seen in this figure, changing the height of the upper patch (h_t), while maintaining all other parameters fixed, both AR and S_{11} are affected. For a smaller height, the AR is optimum near the FCC band, whereas for the larger height, the AR becomes optimum near the ETSI band. In addition, by increasing the height of the upper patch, the bandwidth of the S_{11} becomes narrower. A compromise between AR and S_{11} is reached for a height of $h_t = 19$ mm.

The sensitivity of the AR and S_{11} in terms of probe location is tested in Fig. 12. The probe feed was placed at three distinct locations measured from the leading edge of the bottom patch. As seen from the figure, the AR is fairly insensitive of feed position; however, the S_{11} is certainly affected by it. Optimum overall response is achieved for d_p somewhere between 15 to 20 mm. The influence of changing the corner truncation size of the bottom patch, $d_{TC,b}$, is illustrated in Fig. 13. Clearly, by increasing the corner truncation size of the bottom patch, the AR frequency response improves; however, the corresponding bandwidth becomes smaller. On the contrary, by increasing the corner truncation size of the bottom patch, the bandwidth of the S_{11} frequency response becomes larger covering the frequency range between 830 to 925 MHz. The final sensitivity test we performed was in terms of the corner truncation size of the upper patch. As seen in Fig. 14, the influence of the corner truncation size of the upper patch on the AR and S_{11} is less profound than the one caused by the lower patch.
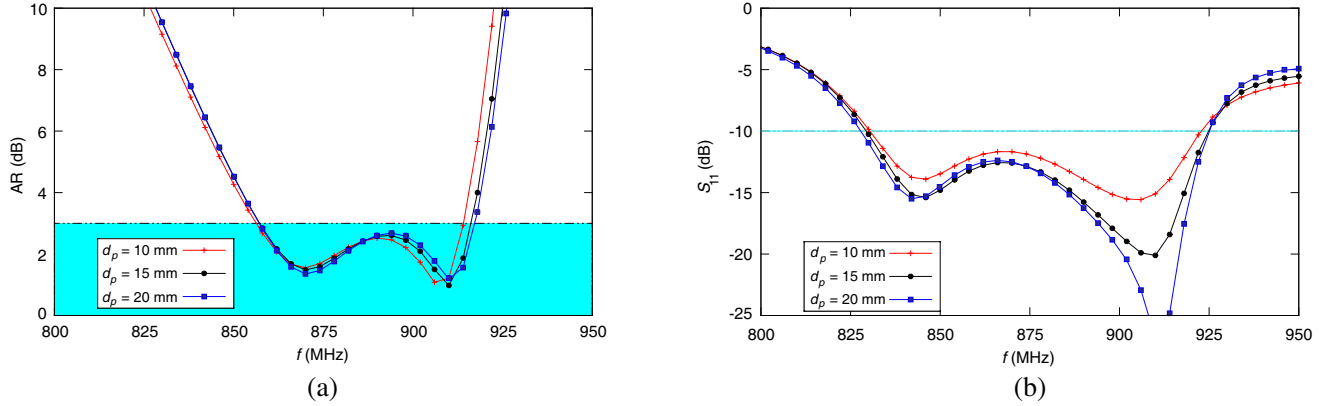
Figure 12. Parametric studies. (a) AR versus frequency for different probe locations relative to the leading edge of the bottom patch. (b) S_{11} versus frequency for different probe locations relative to the leading edge of the bottom patch. ($W_s = L_s = 20$ mm, $h_b = 7$ mm, $h_t = 19$ mm, Bottom patch: 160×160 mm^2 and $d_{TC,b} = 36$ mm; Top patch: 142×142 mm^2 and $d_{TC,t} = 21$ mm).
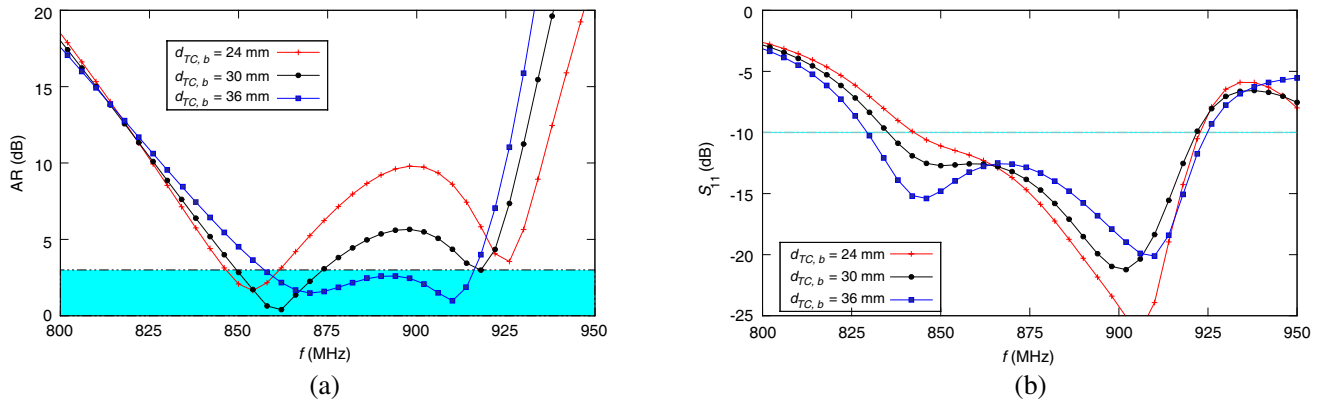
Figure 13. Parametric studies. (a) AR versus frequency for different truncation sizes for the bottom patch. (b) S_{11} versus frequency for different truncation sizes for the bottom patch. ($W_s = L_s = 20$ mm, $h_b = 7$ mm, $h_t = 19$ mm, Bottom patch: 160×160 mm^2 and probe location equal to 15 mm from leading edge; Top patch: 142×142 mm^2 and $d_{TC,t} = 21$ mm).
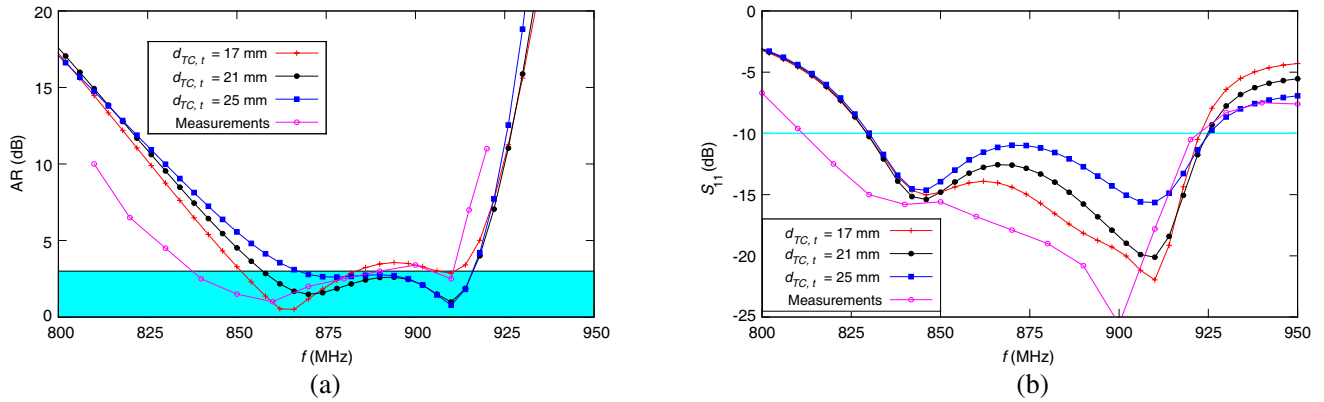
Figure 14. Parametric studies. (a) AR versus frequency for different truncation sizes for the top patch. (b) S_{11} versus frequency for different truncation sizes for the top patch. ($W_s = L_s = 20$ mm, $h_b = 7$ mm, $h_t = 19$ mm, Bottom patch: 160×160 mm^2, $d_{TC,b} = 36$ mm, and probe location equal to 15 mm from leading edge; Top patch: 142×142 mm^2).

By increasing the corner truncation size of the upper patch, the optimum AR shifts from the ETSI to the FCC band; the compromised AR frequency response corresponds to a truncation size of 21 mm. In terms of the S_{11}, increasing the corner truncation size of the upper patch, the corresponding frequency response worsens. Consequently, the optimum stacked-patch design with truncated corners is the one shown in Table 1. In Fig. 14, we also show the measurements performed in the laboratory in order to verify the final design. As seen from the comparison, the measurements closely follow the simulations results for both AR and S_{11}. Measurements were also performed for the normalized radiations patterns (E_ϕ) at 865 MHz in the E- and H-planes. As shown in Fig. 15, there is a very good agreement between simulation results and measured data.

The overall efficiency of the stacked-patch antenna was also computed using ANSYS HFSS and the result is illustrated in Fig. 10. As there are no dielectric or conduction losses associated with the antenna design, this efficiency plot effectively represents the percentage of the accepted power over the input power to the antenna's port. As shown, the antenna efficiency is higher than 94% for a wide frequency band covering almost all the range of interest. This high efficiency provides an important advantage over similar works that appear in the literature mainly due to the lack of lossy substrates and good impedance matching.

Table 2. Comparison of wideband UHF antennas for RFID reader applications.

Antenna Design	AR bandwidth (MHz)	RL bandwidth (MHz)	Dimensions ($L \times W \times h$) mm^3	Gain (dBic)	Geometrical Complexity
This work	855–918	830–925	$200 \times 200 \times 19$	9.3	2 stacked patches (air)
Ref. [6]	818–964	760–963	$250 \times 250 \times 35$	8.3	3 stacked patches (FR4, air)
Ref. [7]	836–986	685–1125	$250 \times 250 \times 60$	8.6	1 patch (FR4, air)
Ref. [8]	835–955	833–1033	$250 \times 250 \times 29.8$	7.0	2 stacked patches (FR4, foam)
Ref. [12]	838–959	758–983	$250 \times 250 \times 36$	8.6	3 stacked patches (FR4, air)
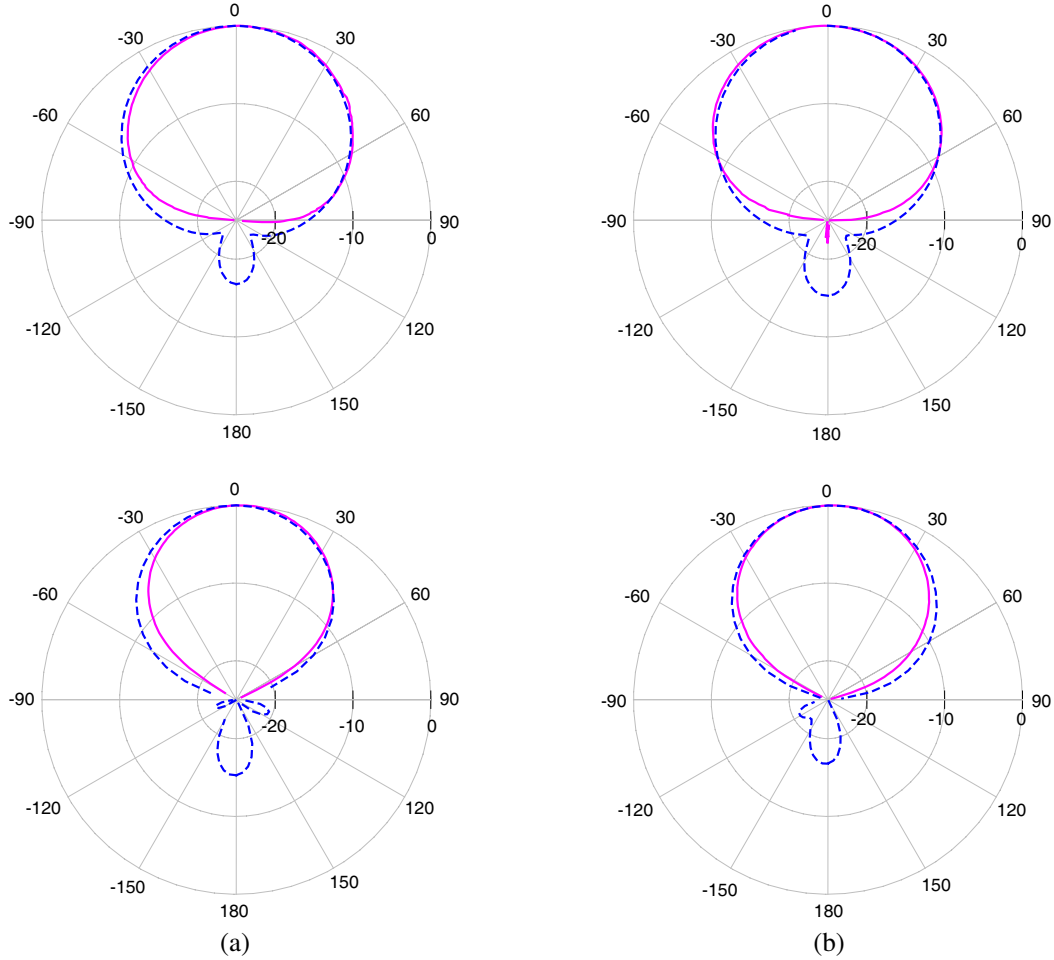
Figure 15. Comparisons between simulations (dash blue line) and measurements (solid purple line) for the normalized radiations patterns (Top: E_ϕ; Bottom: E_θ) at 865 MHz in the E- and H-planes of the double-patch antenna. (a) E-plane elevation pattern (z-y plane); (b) H-plane elevation pattern (z-x plane).

The stacked-patch antenna has been tested in a realistic environment using an RFID reader by Impinj and Dogbone UHF tags made by Smartrac. The input power to the reader was 30 dBm and the maximum reading range at boresight and for tags hanging in free space was 11 m. The corresponding maximum reading range for an MTI commercial antenna MT-242032/NRH (865–870 MHz, 7 dBic) was 6 m, whereas for the broadband commercial design published in [5] was 10 m. Due to the improved reading range observed in the current work, we managed to obtain a better coverage for our healthcare project using reduced number of networked antennas within the pharmaceutical warehouse.

A comparison of the stacked-patch antenna with similar designs that are already published in the open literature is provided in Table 2. As observed from the comparison, the proposed antenna is a two-layer stacked patch antenna design as opposed to a three-layer patch antenna design published in [6, 12]. In addition, the proposed design does not utilize FR4 substrates, which are highly lossy and adversely affect the gain and efficiency of the antenna. Concerning the designs published in [7] and [8], even though they correspond to a single-layer and two-layer stacked patch design, respectively, they also involve use of FR4 substrates. Furthermore, the single-layer design in [7] exhibits a gain of 8.6 dBic, whereas the two-layer design in [8] is characterized by the lowest overall gain (7 dBic). The design proposed in this paper exhibits the highest overall gain which is 9.3 dBic, something which justifies the large reading range observed when testing this particular antenna in a realistic environment. Finally, the height of the proposed design is the smallest of all (19 mm) which is suitable for a non-bulky antenna package.

3. CONCLUSIONS

In this work, we have managed to design and build single-feed, truncated-corner, air-filled patch antennas for UHF RFID application suitable for operation in the ETSI and FCC frequency bands. It was observed that the use of a stack of two patches, both with truncated corners at a 45-degree angle, can lead to an optimized design that sufficiently covers both ETSI and FCC UHF RFID bands with attractive AR and S_{11} frequency response. In addition, this stacked-patch design exhibits high gain (9.3 dBic) and radiation patterns with high beamwidths and low back radiation. Through a number of parametric studies, we identified the mechanisms that can tune the antenna characteristics in order to reach an optimum design within the frequency band of interest.

REFERENCES

1. Finkenzeller, K., *RFID Handbook: Fundamentals and Applications in Contactless Smart Cards and Identification*, Wiley, New York, 2004.

2. Polycarpou, A. C., A. Dimitriou, A. Bletsas, P. C. Polycarpou, L. Papaloizou, G. Gregoriou, and J. N. Sahalos, "On the design, installation, and evaluation of a radio-frequency identification system for healthcare applications," *IEEE Antennas Propag. Magazine*, Vol. 54, No. 4, 255–271, 2012.

3. Sharma, P. C. and K. C. Gupta, "Analysis and optimized design of single feed circularly polarized microstrip antennas," *IEEE Trans. Antennas Propag.*, Vol. 31, No. 6, 949–955, 1983.

4. Sim, C.-Y.-D. and C.-J. Chi, "A slot loaded circularly polarized patch antenna for UHF RFID reader," *IEEE Trans. Antennas Propag.*, Vol. 60, No. 10, 4516–4521, 2012.

5. Li, J., Y. Huang, Y. Wang, Q. Zhang, G. Wen, and H. Zhang, "Widebang high gain circularly polarized UHF RFID reader antenna," *2016 IEEE Conference on Antenna Measurements and Applications (CAMA)*, 1–3, 2016.

6. Chen, Z. N., X. Qing, and H. L. Chung, "A universal UHF RFID reader antenna," *IEEE Trans. Microw. Theory Techn.*, Vol. 57, No. 5, 1275–1282, 2009.

7. Sim, C.-Y.-D., Y.-W. Hsu, and G. Yang, "Slits loaded circularly polarized universal UHF RFID reader antenna," *IEEE Antennas Wireless Propag. Lett.*, Vol. 14, 827–830, 2015.

8. Nasimuddin, Z. N. Chen, and X. M. Qing, "Asymmetric-circular shaped slotted microstrip antennas for circular polarization and RFID applications," *IEEE Trans. Antennas Propag.*, Vol. 58, No. 12, 3821–3828, 2010.

9. Lee, J. M., N. S. Kim, and C. S. Pyo, "A circular polarized metallic patch antenna for RFID reader," *Proc. Asia-Pacific Commun. Conf.*, 116–118, Perth, WA, 2005.

10. Kovitz, J. and Y. Rahmat-Samii, "Using thick substrate and capacitive probe compensation to enhance the bandwidth of traditional CP patch antennas," *IEEE Trans. Antennas Propag.*, Vol. 62, No. 10, 4970–4979, 2014.

11. Wu, J., X. Ren, Z. Wank, and Y. Yin, "Broadband polarized antenna with L-shaped strip feeding and shorting-pin loading," *IEEE Antennas Wireless Propag. Lett.*, Vol. 13, No. 9, 1733–1736, 2014.

12. Wang, Z., S. Fang, S. Fu, and S. Jia, "Single-fed broadband circularly polarized stacked patch antenna with horizontally meandered strip for universal UHF RFID application," *IEEE Trans. Microw. Theory Techn.*, Vol. 59, No. 4, 1066–1073, 2011.

13. Herscovici, N., Z. Sipus, and D. Bonefacic, "Circularly polarized single-fed wire-band microstrip patch," *IEEE Trans. Antennas Propag.*, Vol. 51, No. 6, 1277–1280, 2003.

14. Chung, K. L. and A. S. Mohan, "A systematic design method to obtain broadband characteristics for singly-fed electromagnetically coupled patch antennas for circular polarization," *IEEE Trans. Antennas Propag.*, Vol. 51, No. 12, 3239–3248, 2003.

15. Yang, W., J. Zhou, Z. Yu, and L. Li, "Single-fed low profile broadband circularly polarized stack patch antenna," *IEEE Trans. Antennas Propag.*, Vol. 62, No. 10, 5406–5410, 2014.

16. Ta, S. X. and I. Park, "Low-profile broadband circularly polarized patch antenna using metasurface," *IEEE Trans. Antennas Propag.*, Vol. 63, No. 12, 5929–5934, 2015.

17. Balanis, C. A., *Antenna Theory, Analysis and Design*, 3rd Edition, Wiley, New Jersey, 2005.